05,10

Effect of Ta and Cu spacer layers on the spin Hall angle in NiFe/Ta/IrMn and NiFe/Cu/IrMn structures

© R.B. Morgunov, M.V. Bakhmetiev

Federal Research Center of Problems of Chemical Physics and Medicinal Chemistry RAS, Chernogolovka, Russia

E-mail: spintronics2022@yandex.ru

Received November 7, 2024
Revised November 20, 2024
Accepted November 21, 2024

The influence of Ta and Cu spacers in NiFe/Ta/IrMn and NiFe/Cu/IrMn structures on the angular dependences of the planar Hall effect (PHE) and the spin current caused by the spin-orbit torque (SOT) was revealed. The studies were carried out in the ranges of electric current and external magnetic field, in which the current and field values do not affect the $R_{PHE}(\varphi_{EX})$ dependences, leaving the exchange bias unchanged. Adding a spacer layer under these conditions reduces the resistance of the planar Hall effect R_{PHE} and affects the spin current generated in the IrMn/Spacer layers. This is expressed in a decrease in the spin Hall angle for NiFe/Ta/IrMn and NiFe/Cu/IrMn with an increase in the thickness of the spacer layer.

Keywords: Spin-orbit torque, exchange bias, spacer, planar and spin Hall effect, spin Hall angle.

DOI: 10.61011/PSS.2024.11.60095.297

1. Introduction

A key strategy for creating logic gates based on antiferromagnets (AFM) is to create an AFM/HM interface with a heavy transition metal (HM), the magnetization of which can change under the impact of the spin Hall effect in a layer of heavy transition metal (Pt, Pd, Ir, etc.) [1–6]. The interaction of spin-polarized electrons with the magnetic moments of the ions of the crystal lattice through spin-orbit coupling leads to the occurrence of a torque (spin-orbit torque, SOT) acting on the spins of the ions of the crystal lattice, as well as to a change of the local orientations of the Neel axes in the antiferromagnet [7–10]. This effect is similar to the behavior of electrons under the action of SOT at the ferromagnetic/heavy metal interface FM/HM [7–10], where SOT occurs due to spin currents generated in the HM layer by the spin Hall effect (SHE). The bulk spin-orbit coupling in HM is caused either by a band structure or by impurities with a large amount of spin-orbit coupling. The spin-dependent asymmetric scattering of conduction electrons takes place in both cases. Asymmetric scattering causes spin-up and spin-down electrons to be deflected in opposite directions and thus creates a transverse spin current when an unpolarized electric current is passed through HM. The polarization σ of the accumulated spins is perpendicular to both the direction of the electric current ($\mathbf{J}_C$) and the direction of the generated spin current ($\mathbf{J}_S$). The density of the transverse spin current SHE can be described by the expression [11]:

$$\mathbf{J}_s = \frac{\hbar}{2e}\theta_{SH}(\mathbf{J}_c \times \boldsymbol{\sigma}), \qquad (1)$$

where θ_{SH} is the spin Hall angle characterizing spin current generation.

Spin-polarized current was studied in the antiferromagnets IrMn, PtMn, and MnN, in metallic two-layer structures [12–14], as well as in structures with a dielectric AFM-layer of NiO [15]. The reorientation of magnetic moments in AFM under the action of an electric field or current demonstrates stable states into which the Neel axes in the spin system of an antiferromagnet can switch at a sufficiently high current density. Switching of the local magnetization in AFM depends on the domain structure, since the SOT induced by the current affects the movement of the domain boundaries. Since the magnetic moment of an antiferromagnet is small, and it is difficult to record changes of magnetic properties under the impact of current, a cover ferromagnetic layer is used as an indicator film sensitive to magnetic transformations in AFM. The magnetic anisotropy, magnetization, and other properties of the FM layer can significantly change when the magnetic ordering in the neighboring AFM layer changes under the action of a spin-polarized electric current [12–15].

Current-induced changes of the exchange displacement in two-layer AFM/FM structures were reported in Ref. [12]. The authors of Ref. [12] have established that the magnitude of the planar Hall effect in NiFe/IrMn changes under the impact of current flowing in the plane of the structure, and retains the current-altered value even after the current is turned off. It is proved that the SOT caused by the spin Hall effect in IrMn effectively reverses the direction of the exchange displacement field. SOT is not directly related to the NiFe ferromagnetic layer, but occurs when the magnetic moments of the antiferromagnet are uncompensated at the NiFe/IrMn interface, where the current stimulates the collective rotation of the magnetization. The crucial role of the interface at which uncompensated AFM moments

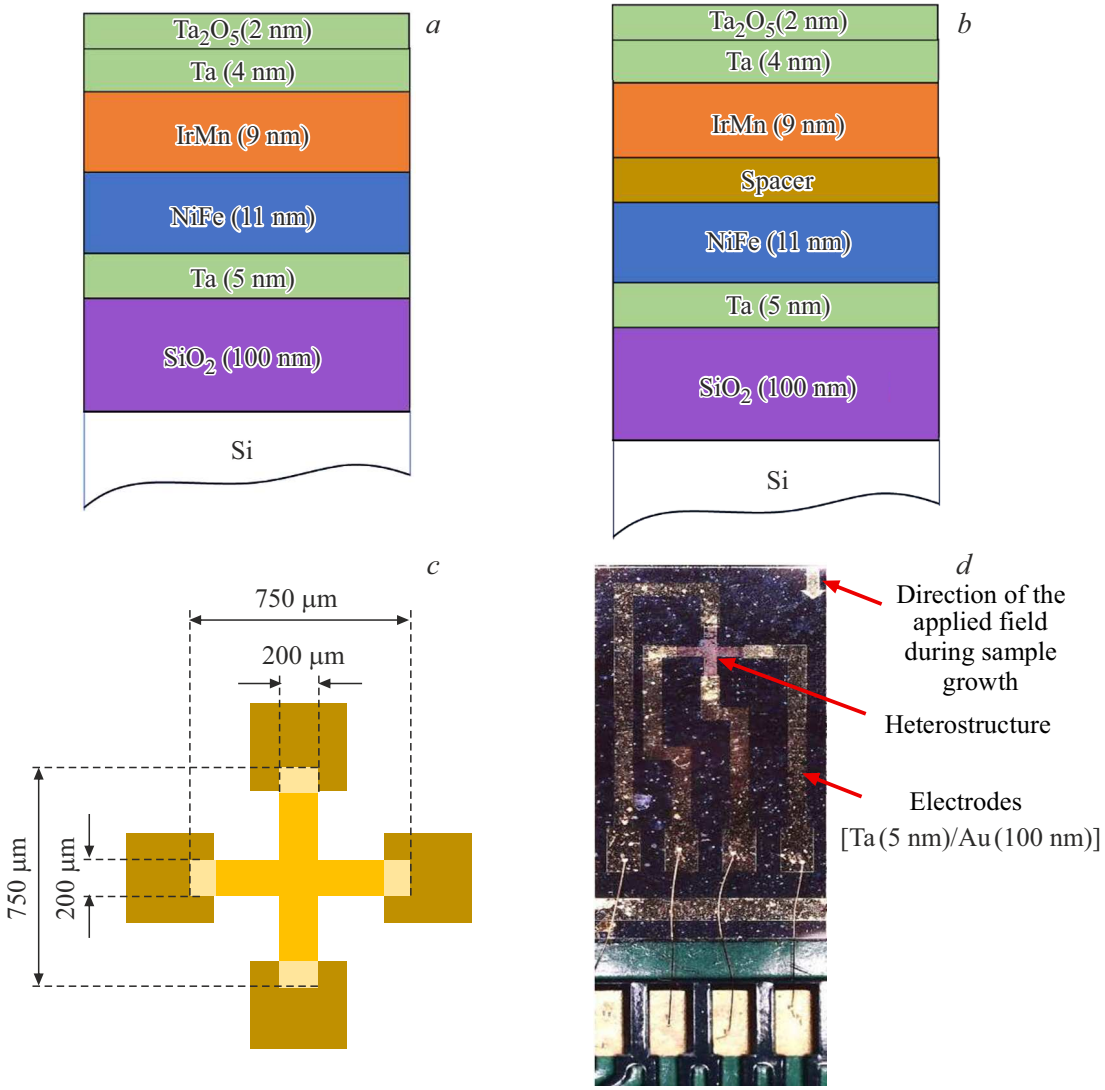

Figure 1. Diagram of samples (*a*) without a spacer interlayer and (*b*) with a Cu or Ta spacer interlayer, (*c*) dimensions of the cruciform sample, (*d*) photo of the „Hall cross“ with contacts connected to the sample for electrical measurements. The arrow indicates the direction of the applied magnetic field during the growth of the sample.

transfer magnetization to exchange-coupled moments in a ferromagnet is proved. It was shown in [16] that AFM can be used for highly efficient magnetization manipulation in the FM layer. An antidumping moment is observed in Ref. [16] that acts on the NiFe ferromagnetic at a plane current in the IrMn antiferromagnetic layer. The Hall spin angle θ_{SH} is significantly higher in the IrMn antiferromagnet than in the heavy transition metals mentioned above. Therefore, we have focused on the study of this material in this paper.

The aim of our study is to determine the Hall spin angle in a sequential series of NiFe/Cu/IrMn and NiFe/Ta/IrMn heterostructures with varying effective thickness of the Cu or Ta spacer nonmagnetic layer, which allows regulating the exchange interaction between NiFe and IrMn up to its complete disappearance.

2. Methodology and samples

Three types of samples were used in the study: one sample type without Ta(5 nm)/NiFe(11 nm)/IrMn(9 nm)/Ta(4 nm)/Ta_2O_5(2 nm) interlayer, the second sample type with a tantalum interlayer between NiFe and IrMn Ta(5nm)/NiFe(11 nm)/Ta(t_{Ta})/IrMn(9 nm)/Ta(4 nm)/Ta_2O_5(2 nm) layers with different thicknesses of tantalum layer t_{Ta}, and the third sample type — with copper interlayer Ta(5 nm)/NiFe(11 nm)/Cu(t_{Cu})/IrMn(9 nm)/Ta(4 nm)/Ta_2O_5(2 nm) (Figure 1, *a, b*) with different thicknesses of layer t_{Cu}.

The samples were fabricated by direct current magnetron sputtering at a base pressure of $2.6 \cdot 10^{-7}$ mTorr, argon pressure of 3 mTorr and gas flow velocity of 30 cm^3/min. The substrates were rotated at a rate of 10 revolutions per minute during sputtering to ensure the uniformity of the

layers. The heterostructures were deposited on Si/SiO_2 substrates. First, a Ta layer was sputterred to buffer the defects and enhance the texture of the subsequent NiFe layer with an orientation (111). The Ta layer also improved the adhesion between the NiFe and IrMn layers and reduced their roughness. Then a spacer layer and IrMn was sputtered, and the final layer of Ta served as protection from the corrosion and oxidation of the layers of NiFe and IrMn. The thickness of the spacer was determined by the magnetron sputtering time. The thickness of the tantalum interlayer varied from 0.1 to 1 nm, which corresponds to the sputtering time from 2 to 30 s. It ranged from 0.2 to 5 nm in case of the copper interlayer, which corresponds to the sputtering time from 2 to 120 s. The choice of the thickness of the separation layers is attributable to the different adhesion of tantalum and copper to the ferromagnetic layer and the different effective thicknesses at which a continuous layer is achieved. In the case of tantalum, a continuous layer is formed with an effective thickness of $t_{Ta} = 0.3$ nm, and $t_{Cu} = 1.3$ nm is required for copper. Therefore, the thickness range is chosen in such a way as to cover the three stages of spacer growth: 1) the formation of individual islands; 2) the formation of a percolation threshold; 3) the formation of a thin continuous layer. The selected thickness range for the two Ta and Cu spacers is different, but covers all three of the above stages.

The sample was prepared for electrical measurements in three stages. Si/SiO_2 substrate was purified in acetone for 1 h at the first stage, then cross-shaped templates were applied using optical lithography. The arms of the cross were of the same size ($200 \times 750\,\mu$m) and mutually perpendicular, as shown in Figure 1, *c*. A heterostructure is grown on the template at the second stage under the conditions described above. The samples were immersed in acetone after sputtering to remove the material sputtered outside the template. A template was first applied at the third stage to connect the contacts to the cross-shaped sample. Then [Ta(5 nm)/Au(100 nm)] layers were sputtered and the procedure of removing excess material in acetone was carried out again. The samples were connected to a printed circuit board using West Bond 7476D paste to supply current and register voltage. Then [Ta(5 nm)/Au(100 nm)] electrodes were connected to the gold contact tracks using micro-welding for subsequent connection to Keithley 6220 current source and Keithley 2182A nanovoltmeter. A photo of connection of the sample to the contacts is shown in Figure 1, *d*. The arrow shows the direction of the applied magnetic field during sample growth. This direction coincides with the direction of the light magnetization axis and the exchange displacement field. The external magnetic field was generated by an electromagnet (Abbess Instruments) and measured with a PCE-MFM 3000 instrument near the sample.

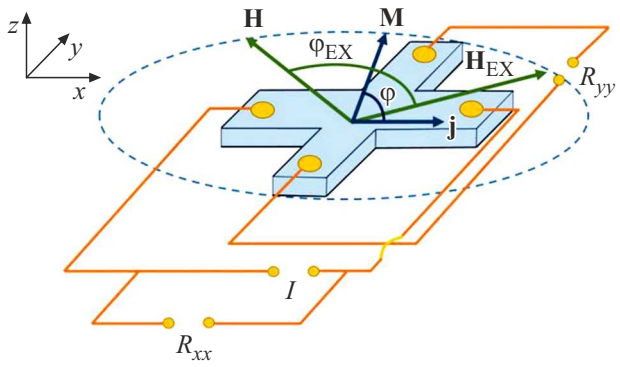

Figure 2. The scheme of measurement of the components of the resistance tensor. The angle φ between the direction of the electric current density **j** and the magnetization **M**, the angle φ_{EX} between the magnetic field **H** and the displacement field directed along the light axis of magnetization $\mathbf{H}_{EX}$.

3. Experimental results and discussion

Electrical measurements were initially aimed at accurately determining the direction of the exchange displacement field. The diagonal components of the resistance tensor in the thin film R_{XX} and R_{YY} correspond to the longitudinal voltage measured along the current direction, while the off-diagonal components R_{XY} and R_{YX} correspond to the transverse voltage [17]. The transverse stress is a planar Hall effect (PHE), while the angular changes in the longitudinal stress correspond to anisotropic magnetoresistance (AMR). All components of the resistance of the thin film vary depending on the angle φ between the direction of the electric current density **j** and the magnetization **M** [18]. The longitudinal and transverse resistances can be expressed by the following formulas at an arbitrary angle φ :

$$R_{AMR} = R_{yy} + (R_{xx} - R_{yy})\cos^2\varphi, \tag{2}$$

$$R_{PHE} = (R_{xx} - R_{yy})\sin\varphi\cos\varphi. \tag{3}$$

The values of the resistances R_{XX} and R_{YY} were determined according to the scheme shown in Figure 2.

The angle φ cannot be determined by direct measurement, since the direction of magnetization *a priori* is unknown. But this angle φ can be calculated, since it depends on the angle φ_{EX} manually set by the goniometer between the magnetic field **H** and the light axis of magnetization. The light axis is parallel to the direction of the exchange displacement field $\mathbf{H}_{EX}$, set by the growth of the sample in the magnetic field, and it coincides with the direction of the sample face (in Figure 1, *d* the arrow indicates the direction of the light magnetization axis). The dependence $\varphi(\varphi_{EX})$ is usually calculated by minimizing the energy E, which includes the energy of magnetic anisotropy (the first term), the Zeeman energy of the ferromagnetic layer in a magnetic field (the second term) and the energy of the exchange interaction between the ferro- and antiferromagnetic layer

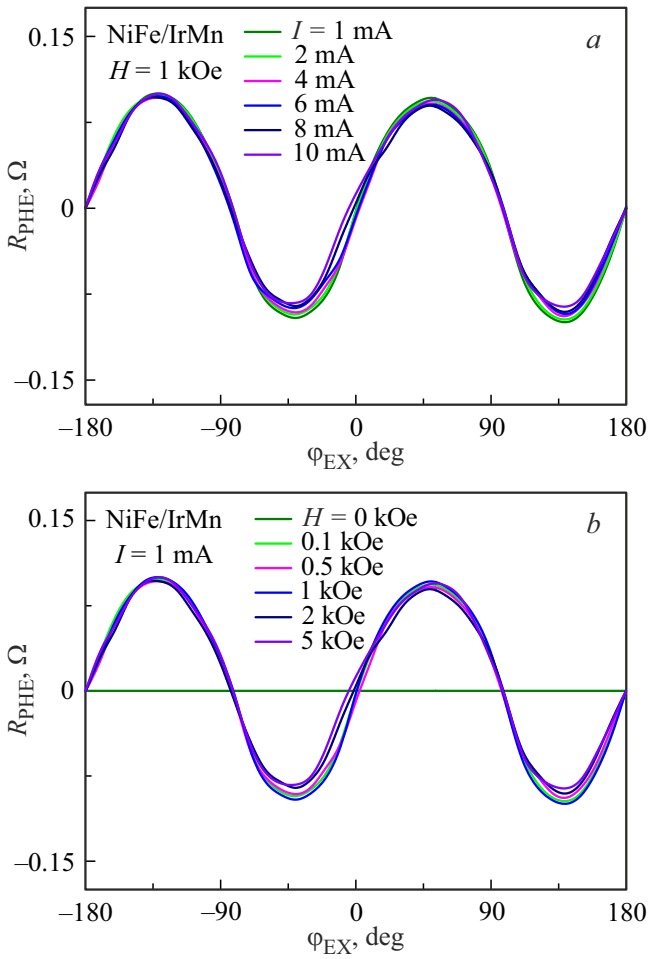

Figure 3. (a) Angular dependence of resistance $R_{PHE}(\varphi_{EX})$ for NiFe/IrMn in direct current $I = 1, 2, 4, 6, 8, 10$ mA. (b) Angular dependence of resistance $R_{PHE}(\varphi_{EX})$ for NiFe/IrMn at DC 1 mA and in different magnetic fields $H = 0, 0.1, 0.5, 1, 2, 5$ kOe.

expressed in terms of the exchange displacement field (the third summand) [19]:

$$E = K_U t_F \sin^2\varphi - M_S t_F H \cos(\varphi - \varphi_{EX}) - M_S t_F H_{EX} \cos(\varphi), \quad (4)$$

where $K_U = (1/2)H_U M_S$ — uniaxial anisotropy constant, H_U — uniaxial anisotropy field, M_S — saturation magnetization, H_{EX} — exchange displacement field, t_F — the thickness of the ferromagnetic layer, $(\varphi - \varphi_{EX})$ — the angle between the magnetization **M** and the magnetic field **H** (Figure 2).

The dependency $\varphi(\varphi_{EX})$ can be expressed analytically using the expressions [18]:

$$\cos\varphi \sim \frac{H_{EX} + H\cos\varphi_{EX}}{\sqrt{H^2\sin^2\varphi_{EX} + (H_{EX} + H\cos\varphi_{EX})^2}}, \quad (5)$$

$$\sin\varphi \sim \frac{H\sin\varphi_{EX}}{\sqrt{H^2\sin^2\varphi_{EX} + (H_{EX} + H\cos\varphi_{EX})^2}}. \quad (6)$$

Substituting experimentally determined resistance components R_{XX} and R_{YY} and calculated angles φ into (3) for each fixed φ_{EX} leads to an angular dependence $R_{PHE}(\varphi_{EX})$. Since, when analyzing angular dependencies, it is important that the dependencies R_{PHE} on current and field are in saturation and the projections of these values do not affect the result (the ferromagnet must be in saturation), we first found out the range of currents and fields in which R_{PHE} does not depend on fields and currents. For this purpose, the angular dependence R_{PHE} was constructed in a constant magnetic field 1 kOe and various currents 1–10 mA (Figure 3, a). In addition, we have constructed angular dependencies $R_{PHE}(\varphi_{EX})$ in various fields $H = 0$–5 kOe (Figure 3, b). Figure 3 shows that the angular dependences did not depend on either the field or the current in the selected range of values of these quantities.

The resistance R_{PHE} was zero minus the background resistance in an external magnetic field **H** parallel or perpendicular to the direction of the exchange displacement field $\mathbf{H}_{EX}$. The resistance of R_{PHE} reaches a maximum value of 0.15 Ω at an angle of $\varphi_{EX} = 45°$.

Therefore, all further measurements were carried out at a current of 1 mA and a magnetic field of 1 kOe. Next, we measured the dependences $R_{PHE}(\varphi_{EX})$ for samples with the addition of a spacer layer of tantalum (Figure 4, a) and copper (Figure 4, b) with different effective thicknesses.

It can be seen that the amplitude of angular variations in resistance R_{PHE} decreases at $\varphi_{EX} = 45°$, both in the case of adding a tantalum interlayer and in the case of a copper one. The dependences R_{PHE} on the thickness of the spacer were constructed in the maximum angular dependence at $\varphi_{EX} = 45°$ (Figure 5).

It follows from Figure 5 that adding a spacer and increasing its thickness reduces the value of R_{PHE}, but does not change the symmetry and angle of maximum angular dependence $\varphi_{EX} = 45°$. This statement is not correct for a copper layer with a thickness of 5 nm, since the angle φ_{EX} for this sample differs from 45° and depends on the effective thickness of the copper layer. At the same time, even the symmetry of the angular dependence itself changes as the thickness of the copper interlayer changes — additional maxima appear.

Next, we obtained the angle of the spin Hall effect for our samples. We use the following expressions to characterize the SOT by the PHE signal and determine θ_{SH}:

$$R_{PHE} = -\frac{\hbar}{eM_s t_{NiFe}} J_s \sin\varphi_{EX}, \quad (7)$$

$$\theta_{SH} = \frac{J_s}{J_c} \cdot 100\%. \quad (8)$$

The magnetization values were preliminarily determined using SQUID magnetometer and are shown in Figure 6 as dependences of the magnetization on the thickness of the spacer layer.

The spin current J_S was determined by approximating the angular dependencies $R_{PHE}(\varphi_{EX})$ with the expression (7)

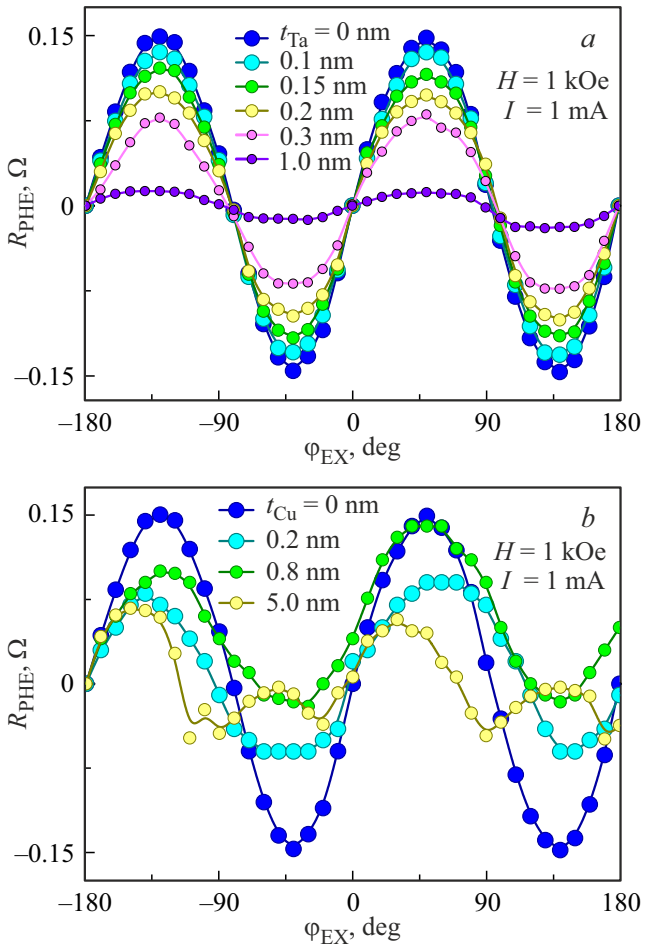

Figure 4. Angular dependence of resistance $R_{PHE}(\varphi_{EX})$ for NiFe/Ta/IrMn (*a*) and NiFe/Cu/IrMn (*b*) at $I = 1$ mA and $H = 1$ kOe for different spacer thicknesses. The lines show the approximation by the expression (7).

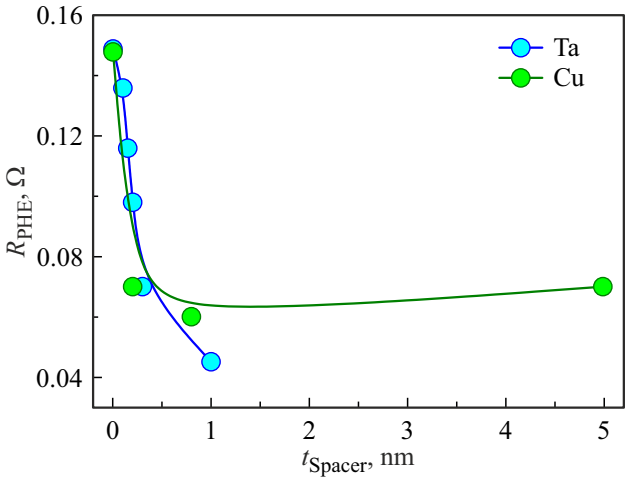

Figure 5. Dependences of the amplitude of the resistance R_{PHE} on its angular dependence at $\varphi_{EX} = 45°$ on the effective thickness of Ta and Cu interlayer.

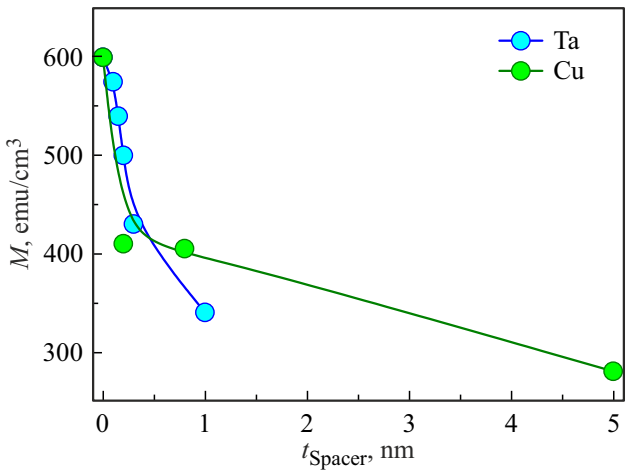

Figure 6. Magnetization dependences normalized for the volume of the NiFe ferromagnetic layer, NiFe/Ta/IrMn and NiFe/Cu/IrMn heterostructures on the thicknesses of Ta and Cu spacers.

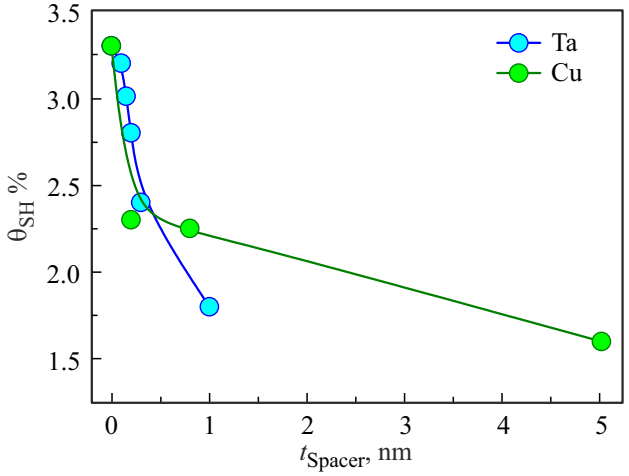

Figure 7. Dependences of the spin Hall angle on the thickness of the Ta and Cu interlayer.

(Figure 4). Knowing the electric current J_C and determining the values of J_S, we calculated the values the spin Hall angle for all spacer thicknesses (Figure 7).

The values of determined θ_{SH} in our paper for the NiFe/Ta/IrMn and NiFe/Cu/IrMn structures range from 1.6 to 3.3%, depending on the material and thickness of the spacer. This limit corresponds to θ_{SH} for IrMn$\theta_{SH} = 1.7-2.7\%$ alloy and for PdMn$\theta_{SH} = 1-2\%$ alloy, but does not reach PtMn $\theta_{SH} = 5-7\%$ [20,21]. The discrepancy may be attributable to the fact that the spin Hall effect signal is usually mixed with undesirable effects associated with the anisotropic magnetoresistance (AMR) effect. The spin Hall angle decreases for both structures containing Cu spacer and structures containing Ta spacer (Figure 7) as the thickness of the spacer interlayer increases, which may be attributable to spin decoherence as the distance traveled by the carrier in a non-magnetic metal increases. The thicknesses of the buffer and protective layer from sample to sample remain unchanged in the studied samples when adding and increasing the thicknesses of Cu

and Ta spacers. The contribution from all layers of the structure without a spacer corresponds to the Hall spin angle for the Ta/NiFe/IrMn/Ta reference sample. The division of this contribution into separate contributions for each layer of the structure has not been carried out.

4. Conclusions

The angular dependences of the planar Hall effect (PHE) and the spin current induced by the spin-orbit moment (SOT) are obtained in the NiFe/Ta/IrMn and NiFe/Cu/IrMn structures. An increase of the thickness of Ta or Cu spacers reduces the spin Hall angle in both types of heterostructures. At the same time, the maximum of the angular dependence does not change its position in structures with tantalum, while the position of the maximum and the symmetry of the angular dependence change in structures with copper. It is established that the magnitude of the electric current and the external magnetic field does not affect the dependences $R_{PHE}(\varphi_{EX})$, leaving the exchange displacement unchanged in the used range of fields and currents. The addition of a spacer layer does not change the direction of the light magnetization axis, but it reduces the resistance R_{PHE} and affects the spin current generated at the IrMn/Spacer interface.

Funding

The work was supported by the thematic map of the Institute of Problems of Chemical Physics and Medical Chemistry of the Russian Academy of Sciences 124013100858-3.

Conflict of interest

The authors declare that they have no conflict of interest.

References

[1] C. Zhou, Y.P. Liu, Z. Wang, S.J. Ma, M.W. Jia, R.Q. Wu, L. Zhou, W. Zhang, M.K. Liu, Y.Z. Wu, J. Qi. Phys. Rev. Lett. **121**, 086801 (2018).
[2] H. Qiu, L. Zhou, C. Zhang, J. Wu, Y. Tian, S. Cheng, S. Mi, H. Zhao, Q. Zhang, D. Wu, B. Jin, J. Chen, P. Wu. Nat. Phys. **17**, 388–394 (2021).
[3] S. Shim, M. Menhaeen, J. Sklenar, J. Oh, J. Gibbons, H. Saglam, A. Hoffmann, S.S.-L. Zhang, N. Mason. Phys. Rev. X **12**, 021069 (2022).
[4] A. Hoffmann. IEEE Trans. Magn. **49**, 5172–5193 (2013).
[5] J.B.S. Mendes, R.O. Cunha, O.A. Santos, P.R.T. Ribeiro, F.L.A. Machado, R.L. Rodriguez-Suarez, A. Azevedo, S.M. Resende. Phys. Rev. B **89**, 140406(R) (2014).
[6] L. Huang, Y. Zhou, H. Qiu, H. Bai, C. Chen, W. Yu, L. Liao, T. Guo, F. Pan, B. Jin, C. Song. Adv. Mater. **34**, 2205988 (2022).
[7] P. Gambardella, I.M. Miron. Phil. Trans. R. Soc. A **369**, 3175–3197 (2011).
[8] R. Ramaswamy, J.M. Lee, K. Cai, H. Yang. Appl. Phys. Rev. **5**, 031107 (2018).
[9] Q. Shao, P. Li, L. Liu, H. Yang, S. Fukami, A. Razavi, H. Wu, K. Wang, F. Freimuth, Y. Mokrousov, M.D. Stiles, S. Emori, A. Hoffmann, J. Akerman, K. Roy, J.-P. Wang, S.-H. Yang, K. Garello, W. Zhang. IEEE Trans. Magn. **57**, 800439 (2021).
[10] C. Song, R. Zhang, L. Liao, Y. Zhou, X. Zhou, R. Chen, Y. You, X. Chen, F. Pan. Prog. Mater. Sci. **118**, 100761 (2021).
[11] J. Sinova, S.O. Valenzuela, J. Wunderlich, C.H. Back, T. Jungwirth. Rev. Mod. Phys. **87**, 1213 (2015).
[12] J. Kang, J. Ryu, J.-G. Choi, T. Lee, J. Park, S. Lee, H. Jang, Y.S. Jung, K.-J. Kim, B.-G. Park. Nature Comm. **12**, 6420 (2021).
[13] J. Zelezny, P. Wadley, K. Olejnik, A. Hoffmann, H. Ohno. Nature Phys. **14**, 220–228 (2018).
[14] M. Dunz, T. Matalla-Wagner, M. Meinert. Phys. Rev. Research **2**, 013347 (2020).
[15] H. Wang, J. Finley, P. Zhang, J. Han, J.T. Hou, L. Liu. Phys. Rev. Appl. **11**, 044070 (2019).
[16] V. Tshitoyan, C. Ciccarelli, A.P. Mihai, M. Ali, A.C. Irvine, T.A. Moore, T. Jungwirth, A.J. Ferguson. Phys. Rev. B **92**, 214406 (2015).
[17] L. Jogschies, D. Klaas, R. Kruppe, J. Rittinger, P. Taptimthong, A. Wienecke, L. Rissing, M.C. Wurz. Sensors **15**, 28665 (2015).
[18] A.D. Henriksen, B.T. Dalslet, D.H. Skieller, K.H. Lee, F. Okkels, M.F. Hansen. Appl. Phys. Lett. **97**, 013507 (2010).
[19] T.Q. Hung, S. Oh, B. Sinha, J.-R. Jeong, D.-Y. Kim, C.G. Kim. J. Appl. Phys. **107**, 09E715 (2010).
[20] W. Zhang, M.B. Jungfleisch, W. Jiang, J.E. Pearson, A. Hoffmann. Phys. Rev. Lett. **113**, 196602 (2014).
[21] I.M. Miron, K. Garello, G. Gaudin, P.-J. Zermatten, M.V. Costache, S. Auffret, S. Bandiera, B. Rodmacq, A. Schuhl, P. Gambardella. Nature **476**, 189 (2011).

Translated by A.Akhtyamov